Journal of Aerosol Science 175 (2024) 106283

Contents lists available at ScienceDirect

Journal of Aerosol Science

journal homepage: www.elsevier.com/locate/jaerosci

Rotating disk diluter hyphenated with single particle ICP-MS as an online dilution and sampling platform for metallic nanoparticles characterization in ambient aerosol

Tianyu Cen [a,b], Laura Torrent [a], Andrea Testino [a,c,*], Christian Ludwig [a,b,**]

[a] Bioenergy and Catalysis Laboratory (LBK-CPM), Energy and Environment Research Division (ENE), Paul Scherrer Institut (PSI), Villigen PSI, 5232, Switzerland
[b] Environmental Engineering Institute (IIE, GR-LUD), School of Architecture, Civil and Environmental Engineering (ENAC), École Polytechnique Fédérale de Lausanne (EPFL), Lausanne, 1015, Switzerland
[c] École Polytechnique Fédérale de Lausanne (EPFL), STI SMX-GE, CH 1015, Lausanne, Switzerland

ARTICLE INFO

Handling Editor: Chris Hogan

Keywords:
Single-particle inductively coupled plasma mass spectrometry
Aerosol metal nanoparticles
Rotating disk diluter
Online measurement

ABSTRACT

The application of single particle inductively coupled plasma mass spectrometry (spICP-MS) for online metallic nanoparticles (NPs) characterization in ambient aerosol remains a challenge. In this study, a hyphenated setup consisting of a rotating disk diluter (RDD) with spICP-MS (RDD-spICP-MS) was used for online sampling and characterization NPs in ambient pressure aerosols. The elemental composition, particle size distribution, and particle number concentration (PNC) of metallic NPs in aerosols could be obtained simultaneously. The RDD allowed sampling of the aerosol at a constant flow rate, adjusting the optimal dilution ratio for characterizing NPs at different PNCs, and exchanging the gas matrix to achieve the requirement of spICP-MS for direct aerosol characterization. In this proof-of-concept study, the feasibility of this setup was tested with AuNPs of different sizes from the argon-based and air-based aerosol. The limit of detection for number concentration is below 30 #/L, which is lower than the regulated environmental level. Moreover, multi-modal samples, as well as the interference of ionic species, were accurately investigated. Finally, AuNPs were spiked with environmental PM10 and Road dust to evaluate the matrix effect as well as the capabilities of the setup to characterize environmental aerosol samples. These results indicate that RDD-spICP-MS has a great potential for online characterization of metallic NPs in the ambient aerosol.

1. Introduction

Engineered nanoparticles (NPs) are widely used in consumer goods, such as paints, textiles, medical plasters, and personal care products (Bolea et al., 2021; Contado, 2015; Laborda, Jiménez-Lamana, Bolea, & Castillo, 2011; Vance et al., 2015; J. Zhao, Lin, Wang, Cao, & Xing, 2020). Because of their wide production, these emerging contaminants can be released into different environmental

* Corresponding author. Bioenergy and Catalysis Laboratory (LBK-CPM), Energy and Environment Research Division (ENE), Paul Scherrer Institut (PSI), Villigen PSI, 5232, Switzerland.
** Corresponding author. Bioenergy and Catalysis Laboratory (LBK-CPM), Energy and Environment Research Division (ENE), Paul Scherrer Institut (PSI), Villigen PSI, 5232, Switzerland.
E-mail addresses: andrea.testino@psi.ch (A. Testino), christian.ludwig@psi.ch (C. Ludwig).

https://doi.org/10.1016/j.jaerosci.2023.106283
Received 21 August 2023; Received in revised form 4 October 2023; Accepted 7 October 2023
Available online 20 October 2023
0021-8502/© 2024 The Authors. Published by Elsevier Ltd. This is an open access article under the CC BY license (http://creativecommons.org/licenses/by/4.0/).

compartments (air, aquatic, and soil) and biological systems (Bacon et al., 2022; Flores et al., 2019; Mozhayeva & Engelhard, 2020). However, the behavior and properties of NPs are dynamic and matrix-dependent, which increases the difficulty of their characterization (Guzman, Finnegan, & Banfield, 2006; Hotze, Phenrat, & Lowry, 2010; Maurer-Jones, Gunsolus, Murphy, & Haynes, 2013; Petosa, Jaisi, Quevedo, Elimelech, & Tufenkji, 2010). For this reason, the development of adequate analytical methodologies is needed. Nowadays, spICP-MS has been used for NPs characterization and quantification in environmental samples (waters and soils) and biological tissues (Abdolahpur Monikh et al., 2019; Rodrigues et al., 2016; Torrent, Laborda, Marguí, Hidalgo, & Iglesias, 2019; Torrent, Marguí, Queralt, Hidalgo, & Iglesias, 2019). Based on this technique, particle size distribution (PSD), particle number concentration (PNC), and elemental composition could be obtained simultaneously at environmentally relevant concentration levels (Bolea et al., 2021; Mozhayeva & Engelhard, 2020). However, the online method for analyzing NPs directly from ambient aerosol by spICP-MS has not been developed yet due to several limitations. Firstly, standard ICP-MS runs with argon plasma, which needs an online gas matrix exchange system to replace the air with argon meanwhile keeping the pressure constant and the flow rate stable in the gas phase. Secondly, when a nebulizer is used, the sample flow rate of the aerosol is controlled by the carrier gas injected with a fixed pressure in the nebulizer located in the introduction system. However, when ambient pressure aerosol is considered, the ICP-MS should directly measure the aerosol without a positive pressure introduction system. Therefore, an extra sampling system is needed to maintain a constant flow and plasma. Thirdly, the PNC should be in an optimal range to achieve appropriate statistics as well as to avoid double events (Abad-Álvaro et al., 2016). Thus, an online dilution system would be useful.

In the literature, the common methodology described for measuring metal-containing aerosols is based on the offline collection (Bilos, Colombo, Skorupka, & Rodriguez Presa, 2001; Quiterio, Sousa da Silva, Arbilla, & Escaleira, 2004; Zereini et al., 2005). Particles are firstly collected on a filter, then acid digested, and finally, the total metal(s) content is measured. Some studies also tried to use liquid extraction for recovering particles from the filter instead of applying an acid digestion process to obtain the particle size information with spICP-MS (Bland et al., 2022; Torregrosa, Grindlay, de la Guardia, Gras, & Mora, 2023). However, with these offline methods, NPs may condense during the sample collection and extraction, forming secondary particles, which complicate or even make their accurate characterization impossible (Fuzzi et al., 2015).

Recently, some online methodologies have been developed for aerosol metal measurements. The combination of filter collection and X-ray fluorescence analysis provides multi-elemental information (Creamean et al., 2016; Rai et al., 2021) during semi-continuous online measurement. The application of microfluidic technologies and electrochemical sensors allows performing quantitative measurements in the field using a recently developed portable device for near-continuous online measurement. (Y.-B. Zhao et al., 2023; Y. B. Zhao, Tang, et al., 2022). Real-time measurements have been achieved by an extractive electrospray ionization source coupled with a time-of-flight mass spectrometer (EESI-TOF-MS) (Giannoukos et al., 2020). Compared to offline methodologies, the aforementioned methods allow direct measurement of metals contained in the aerosol avoiding the commonly used sample pretreatment steps (e.g. liquid quench or microwave digestion). In addition, with the increase of the time resolution range from hours to seconds, the methods gradually evolve from semi/near-continuous measurement into continuous measurement. Nevertheless, none of these technologies works in single particle mode, due to higher limits of detection or long sampling and measurement times.

In the literature only a few preliminary studies report on the use of ICP technologies for the online elemental analysis of aerosols. Before spICP-MS was available for aerosol characterization, ICP-MS was coupled to a differential mobility analyzer (DMA) for the particle size selection and further determination of the elemental composition (Foppiano, Tarik, Gubler Müller, & Ludwig, 2018a; 2018b; Hess, Tarik, & Ludwig, 2015, 2016; Tarik, Foppiano, Hess, & Ludwig, 2017). One of the limitations of this setup is that the size resolution could not reach the single particle level, and also it is not possible to distinguish metallic from ionic salt particles.

In addition to selecting the particle size, DMA has been also used as a gas converter to replace the matrix from air to argon (Myojo, Takaya, & Ono-Ogasawara, 2002). After the matrix replacement by sheath gas, the aerosol sample could be directly characterized in ICP-MS. The limitation of this method is the cutoff size of the DMA which is smaller due to the low breakdown voltage of argon compared to air. After the rise of applications using spICP-MS, recently more researchers have used a gas exchange device (GED) to convert the sample gas matrix to argon, which is required to operate the plasma (Duelge, Mulholland, Bustos, Zachariah, & Pettibone, 2022; Ohata, Sakurai, Nishiguchi, Utani, & Günther, 2015; Ohata & Nishiguchi, 2017; Tan et al., 2016). With a double-layer concentric glass tube, the sample flow in the inside channel is exchanging the gas matrix with the argon flow at the outside channel via diffusion. A DMA-GED-spICP-MS setup gives a two-dimension particle size distribution of NPs from both DMA and spICP-MS to obtain the aggregate state of AuNPs (Hsieh, Lin, Hsiao, & Hou, 2022; Tan et al., 2016, 2019). However, often in real environmental aerosol samples, such as an off-gas from an engine, the PNC is too high to perform spICP-MS measurements. The rotating disk diluter (RDD) is another versatile option that can be used to adjust the concentration and exchange the gas matrix (Hess, Tarik, Losert, Ilari, & Ludwig, 2016). By adjusting different rotating speeds, the dilution gas dilutes NPs in the aerosol in a wide concentration range. The coupling of DMA-RDD-spICP-MS has recently been reported for characterizing AuNP aggregation after sintering (Bierwirth, Olszok, Wollmann, & Weber, 2022).

These researches have provided several solutions for direct aerosol metal analysis. Up to now, the application of spICP-MS in direct aerosol characterization mainly focused on pure monodisperse metallic NPs. However, in environmental samples, the effect of the matrix, the particle mixtures, and the ionic interferences must be considered. This has not been thoroughly investigated so far. In addition, the previous setup was working with an overpressure aerosol generation system without an aerosol sampling unit. When aerosol was generated, the carrier gas controlled by the mass flow controller (MFC) carries the sample through the setup until it reaches the plasma (Bierwirth et al., 2022; Foppiano et al., 2018a; Tan et al., 2016). However, when aerosols are passed through a unit with a high pressure drop like in a DMA, it causes a flow rate loss at the unadjusted initial overpressure and further falsifies the aerosol characterization (Y. B. Zhao, Cen, et al., 2022). Moreover, analyzers which that do not suck the aerosol for sampling, are generally not suitable for aerosol measurements at ambient or low pressures. For aerosol measurements, pumps should not be installed before the

analyzer to avoid losses or contamination from the pump. Therefore, a new design for the sample introduction system is needed that allows an appropriate hyphenation with the detector unit.

In this paper, an aerosol generator (AG) was used to generate aerosols containing AuNPs in different matrices. After a silica dryer, a T-junction connection was applied to release the excess aerosol into the open air at ambient pressure (Fig. 1). The RDD together with a vacuum pump was connected for sampling independently of the aerosol generation process. With the negative pressure provided by a vacuum pump, the sample flow rate can be adjusted to overcome the pressure drop of RDD without affecting the aerosol generation at the initial pressure in the AG. Based on the adjustable speed of RDD, the whole system worked under different dilution ratios of the aerosol. The spICP-MS was employed to characterize and quantify NPs present in aerosols. For the investigations, a model aerosol containing AuNPs generated with an AG was used. The capabilities of the analytical setup to resolve the PSD and to distinguish metallic AuNPs intensities from ionic interferences were assessed. Finally, the analytical methodology was tested in complex environmental matrices, using PM10 and road dust samples spiked with AuNPs.

2. Material and methods

2.1. Chemicals

Citrate-stabilized bared AuNPs with sizes of 40 (39 nm ± 4), 60 (58 nm ± 5), 80 (83 nm ± 8), and 100 nm (99 nm ± 10) purchased from Nanocomposix (USA) were used as standard particles. Different sized polystyrene latex spheres (40, 60, 80, and 100 nm) purchased from Thermo Scientific (USA) were employed for scanning mobility particle sizer (SMPS) calibration. For the mixture experiments with AuNPs and ionic gold, an ionic gold ICP standard (Sigma-Aldrich, USA) with an initial concentration of 1000 mg Au^{3+}/L was employed. Milli-Q ultrafiltrated and UV-treated water (18.2 MΩ cm, Arium Pro VF Sartorius, Germany) was used for diluting the particle suspensions to 10^6 #/mL. Argon with a 99.999% purity (PanGAS, Swiss) was used for ICP measurements.

2.2. Setup description

The hyphenated setup (RDD-spICP-MS) is presented in Fig. 1. The AuNPs suspension containing NPs of different sizes was diluted to 10^6 #/mL with Milli-Q water in the reservoir of the AG. An AG (TOPAS ATM220, Germany) was employed as an independent aerosol generation system, which was operated at 1 bar (gauge pressure) using argon or air to generate the aerosol. The flow passed through a silica gel dryer column (TOPAS, Germany) to remove the water and a T-junction was connected to release the overpressure aerosol into the open air. A vacuum pump after the RDD was operated to maintain a stable sample flow rate of 0.9 L/min, overcoming the pressure drop at RDD. The flow rate was accurately measured by a primary flow calibrator (Gilibrator 2, Sensidyne, USA). The RDD (MD193E, Testo, Germany) system, which was used before the ICP-MS, allowed the online dilution of the NPs and the gas exchange of the initial process gas, e.g. air, with the target process gas, e.g. Ar. To avoid condensation, the RDD was maintained at 80 °C. After the gas exchange in the rotating disk, an additional flow of argon (0.9 L/min), which was controlled with an MFC, flushed the diluted samples to ICP-MS. An ICP-MS 7700x (Agilent Technologies, Japan), was used in single-particle mode, worked without the nebulizer system and provided the PSD, PNC, and the elemental composition of the NPs. The operation conditions of the ICP-MS were checked before every measurement by adding a flow of 4 mL/min Xe/Ar mixture (100 mg/mL Xe) before the ICP-MS inlet. The monitoring of ^{124}Xe

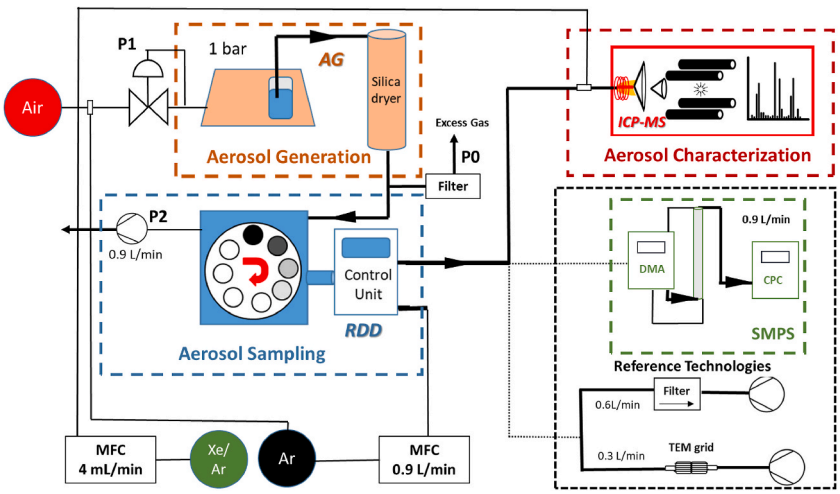

Fig. 1. Schematic representation of the proposed coupled method (RDD-spICP-MS) for online sampling, dilution, and characterization of metallic NPs in the aerosol. AG: aerosol generator, RDD: rotating disk diluter, and ICP-MS: inductively coupled plasma mass spectrometry working in single particle mode. DMA: differential mobility analyzer, CPC: condensation particle counter, SMPS: scanning mobility particle sizer, and TEM: transmission electron microscopy are used as reference technologies.

allowed the detection of any drift of the signal during the analysis (Foppiano et al., 2018a). The measurement conditions of the ICP-MS are summarized in Supporting Information (Table S1). Compared to the previous coupling setup of DMA-GED-spICP-MS (Tan et al., 2016) and DMA-RDD-spICP-MS (Bierwirth et al., 2022), our setup can run at self-sampling mode because no overpressure is needed to inject the sample into the setup.

2.3. Setup calibration

For spICP-MS, the calibration allows finding out the relationship between peak intensity distribution and the mass of the particles contained in the standards, as well as the relationship between peak frequency and number concentration of the particles present in the standards. Usually, there are two common approaches for calibration (Meermann & Nischwitz, 2018): by using 1) NP standards of known size (Laborda et al., 2011), or 2) using transport efficiency and ionic standard solution (Pace et al., 2011). In this project, the transport efficiency method was not feasible. This fact is mainly because of the difference between the spICP-MS working in liquid mode and our RDD-spICP-MS coupling system working in aerosol mode. Compared to the nebulizer system, the AG works without a peristaltic pump to do the sample uptake and drain. Therefore, it is unreachable to obtain the sample uptake rate for calculating the transport efficiency (Tan et al., 2016). Moreover, to measure the aerosol at ambient pressure, a T-junction was designed to separate the aerosol generation from the aerosol sampling process. This process also complicated the transport efficiency calculation since not all the aerosol generated from the liquid was sampled for spICP-MS characterization.

For particle mass calibration, we used standard-sized AuNPs from 40 nm to 100 nm (Bierwirth et al., 2022; Laborda et al., 2011; Tan et al., 2016). The details of data processing related to particle size calibration including the limit of detection for size (LOD_{size}) and number (LOD_N) are described in SI (section 2, with Fig. S1). In addition, the shape of the NPs in the aerosol was characterized by TEM to correctly transfer the particle mass into equivalent size. To do this, the AuNPs in the aerosol were collected by a TEM grid (Fig. 1). The details of the TEM collection methodology and data analysis are described in SI (section 3, with Fig. S2).

For PNC calibration, the relationship between the initial PNC in raw aerosol and the peak frequency given by spICP-MS was used. Without the dilution process, the PNC should be the same from sampling before the RDD until the ICP-MS detector (Bierwirth et al., 2022). However, in the proposed system an online dilution process was taking place, hence a calibration based on the dilution system (RDD) was needed to calculate back the initial PNC in the raw aerosol. To calibrate the RDD in argon mode, an SMPS (SMPS 2100, Palas, Germany) system consisting of a differential mobility analyzer (DMA) and a condenser particle counter (CPC) replaced the ICP-MS (Fig. 1).

Normally SMPS works in an air matrix. In this case, for switching the SMPS working conditions from air to argon, 4.5 L/min of argon was flushed through the system for 2 h. Afterward, 0.9 L/min and 4.5 L/min were set as the sample flow rate and sheath gas flow rate, respectively. The size after the correction was validated with the standard-sized polystyrene latex spheres. The RDD system can be tuned from 10% to 100% by a potentiometer that sets the disk rotation speed (where 10% is more diluted and 100% is less diluted). In addition, different cavity disks exist for different dilution ranges. Thus, the number of cavities present in the rotating disk defines the dilution ratio (DR). There are two types of rotating disks: 10 and 8 cavities. The 10 cavities disk is used to obtain DRs from 1:15 to 1:150 and the 8 cavities disk is used for DRs from 1:150 to 1:1500. The calibration of each rotating disk was based on a previous calibration method (Hueglin, Scherrer, & Burtscher, 1997). First, the raw aerosol concentration and the diluted aerosol concentration were measured in the range of 10%–100% (step 10%) using Milli-Q water as blank. Since the size determination by SMPS will not be influenced by the particle composition and density, a 0.1 wt% NaCl solution was employed as a standard aerosol with a broad size distribution (Y. B. Zhao, Cen, et al., 2022). The measurements were carried out with and without RDD. For each measurement, the DMA was programmed to scan for 180 s in a particle size range from 10 nm to 200 nm. Then, the CPC recorded the signal and the PSD was derived. Each measurement was repeated three times. With these measurements, the DR at each potentiometer position and for each NP size was calculated by using Equation (1):

$$DR = \frac{N_{dil} - BLK_{dil}}{N_{raw} - BLK_{raw}} \quad \text{Equation 1}$$

where N_{dil} is the NaCl PNC after RDD, N_{raw} is the NaCl PNC without RDD, BLK_{dil} is the Milli-Q water PNC after RDD, and BLK_{raw} is the Milli-Q water PNC without RDD.

On the other side, the limitation of using standards of known NPs sizes as the calibration method can be recognized since not all the elements have the standard particles available. In the literature, some studies have tried to do the calibration of P, As, and Hg directly in aerosol with a standard gas stored in a gas cylinder (Ohata et al., 2015; Ohata & Nishiguchi, 2017). This method could not be widely used for other elements due to the high toxicity of these standard gases as well as the limited availability of gaseous metal standards.

2.4. Application of RDD-spICP-MS for air-based aerosol characterization

A preliminary study was carried out to validate the setup running in air-based aerosol. In this case, AG produced the air-based aerosol of 100 nm AuNPs generated from an initial concentration of $5{\cdot}10^6$ #/mL for calibration standard. Both 8 cavities and 10 cavities RDD were used to figure out the influence of air on PSD and PNC determination at a larger range of dilution ratios. Since the matrix switches from argon to air, the LOD_{size} was corrected using Xe as the internal standard as shown in Equation (2). Then LOD_N at each DR was calculated by the same method from Equation S2.

$$LOD_{size,air} = LOD_{size,argon} \times \left(\frac{I_{Xe,argon}}{I_{Xe,air}}\right)^{\frac{1}{3}}$$ Equation 2

where $I_{Xe,\ argon}$ is the ^{124}Xe intensity with pure argon matrix, and $I_{Xe,\ air}$ is the ^{124}Xe intensity with air matrix at different DR. $LOD_{size,argon}$ is the LOD of AuNP size with pure argon matrix at different DR. $LOD_{size,air}$ is the LOD of AuNP size with air matrix at different DR.

2.5. RDD-spICP-MS for mixtures of different sized AuNPs and ionic Au^{3+}

In the atmosphere, the existence of metals in aerosols is usually in a complex form, e.g. metal salts, metal clusters, and metallic NPs. These forms cannot be easily analyzed or physically separated (Moreno et al., 2006). This also makes it difficult to assess the toxicological effects of complex metal aerosol mixtures (Egorova & Ananikov, 2017). When working with traditional methods like SMPS, only the overall PSD can be obtained. Therefore, the PSD of metal salt particles and metallic NPs cannot be distinguished. The application of spICP-MS partially solves the problem since the metal NPs (individual peaks) and the metal salts (stable ionic background) can be differentiated. However, with the increase in ionic salt concentration, the overall increase in noise-to-signal ratio also increases the LOD of the system (Schwertfeger et al., 2017). To investigate the performance of the setup concerning distinguishing between different-sized AuNPs, 40 nm AuNPs were mixed with 60, 80, and 100 nm AuNPs at the same number concentration of 10^6 #/mL. In addition, to check the influence of ionic species present in the aerosol, a test was carried out by mixing 40, 60, 80, or 100 nm AuNPs at 10^6 #/mL with Au^{3+} of an equivalent mass concentration in the AG reservoir.

2.6. RDD-spICP-MS working in environmental aerosol matrices

To test the applicability of the developed RDD-spICP-MS for environmental aerosol characterization, two Certified Reference Materials (CRMs) including PM10-like powder and road dust (IRMM, Belgium) were spiked with AuNPs. For preparing both environmental samples, 0.15 g of powder was weighed and suspended in 50 mL Milli-Q water. Then, the samples were shaken with a vortex (uniTEXER, LLG Labware, Germany) at 1000 rpm for 5 min, followed by sonication in a water bath (Retsch, Germany) for 30 min (35 kHz). After that, 1 mL of each sample was diluted with 50 mL Milli-Q water and spiked with AuNPs of 40 or 100 nm at 10^6 #/mL. Then, the samples were analyzed with the developed RDD-spICP-MS method for determining the AuNPs PSD. Three replicates of each sample were measured at each RDD potentiometer position.

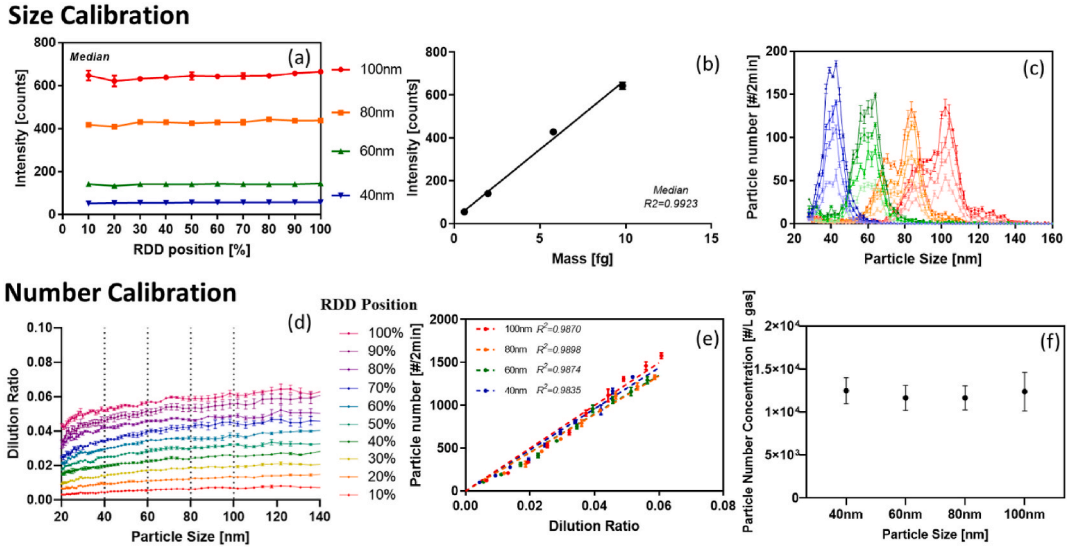

Fig. 2. The size and the NP number calibration of RDD-spICP-MS setup. (a) The median intensity of single particle signal in spICP-MS for different sized AuNP standards at each RDD position after removing data below LOD. (b) The calibration curve shows single particle intensity as a function of mass. (c) The particle size distribution (PSD) of 40 (blue), 60 (green), 80 (orange), and 100 nm (red) AuNP at different RDD positions (40, 60, 80, and 100% from lighter to darker for the same color) after size calibration. (d) The dilution ratio for different sized particles at different RDD positions. (e) The particle number of each sized AuNP counted in spICP-MS at each DR. (f) The particle number concentration (PNC) of each sized AuNP in the aerosol measured after calibration. ANOVA test indicated no statistical difference in PNC among different sized AuNPs. (For interpretation of the references to color in this figure legend, the reader is referred to the Web version of this article.)

3. Results and discussion

3.1. RDD-spICP-MS for argon-based aerosol measurements

Different-sized AuNPs resulted in different intensities obtained from spICP-MS measurements (Fig. S3). For each sized AuNP, the peak positions (Fig. S3), as well as the median intensity (Fig. 2a), were at the same level among different dilution ratios. This indicates that the online dilution process with the RDD does not affect the particle mass and size determination. An acceptable linearity was obtained ($Y = 64.89X+23.15$, $R^2 = 0.9923$) between the median intensity and AuNP mass at each particle size (Fig. 2b). By confirming the spherical particle shape of the AuNPs via TEM (Fig. S2), the intensity distribution could finally be transferred into PSD (Fig. 2c). For each sized AuNP, the LOD_{size} (from Equation S1) was always around 25 nm, showing that the background level is at the same level for different sized AuNPs in the absence of ionic Au. For AuNPs of 40 and 60 nm, the PSD followed a monomodal distribution; for bigger AuNPs of 80 and 100 nm, a second size peak could be found in the distribution. This phenomenon may be due to manufacturer rather than double events. Compared to the manufacturer certified values the particle sizes obtained by a RDD-spICP-MS were similar to the TEM (Table S2). The PSDs obtained by RDD-spICP-MS were broader than TEM, which may be attributed to the occurrence of particles partially detected in spICP-MS during a specific dwell time (Laborda, Jiménez-Lamana, Bolea, & Castillo, 2013). In previous literature, researchers stated the risk of having double events when working with long integration times and with high PNC (Hineman & Stephan, 2014; Montaño, Badiei, Bazargan, & Ranville, 2014), which needed further dilution. Therefore, RDD was applied for online dilution to minimize the effect of high PNC. Since no shift of the distribution was found at different dilution ratios (Fig. 2c), we confirmed that the issue did not come from the double events.

After the size calibration, the NP number calibration was done to calculate the initial number concentration of AuNP in the raw aerosol before RDD. As it is shown in Fig. 2d, the DR at each RDD position first increases with the particle size and then gradually gets stable. This indicates more particle loss at a smaller size range, which is due to diffusion losses (Ayala, Olson, Cantrell, Drayton, & Barsic, 2003). When selecting the particle size (40, 60, 80, and 100 nm), the DR of each particle size was calculated by using Equation (1). A linear relationship could be found between the particle number counted by spICP-MS and the DR at each RDD position (Fig. 2e), indicating that all positions in RDD fulfill the number concentration requirement for spICP-MS characterization. Therefore, the LOD_N can be calculated minimum at 27.8 #/L gas based on Equation S2 when applying maximum DR. In addition, the slope of the curve in Fig. 2e is exactly the particle number in aerosol before the dilution. Fig. 2f shows that the calculated PNC in the raw aerosol for 100, 80, 60, and 40 nm AuNPs was all around $1.2{\cdot}10^4$ #/L gas based on Equation S3. An analysis of variance (ANOVA) showed no obvious difference in the number concentration among different-sized particles in the aerosol ($P > 0.05$). This demonstrates the reliability of the calibrated system for characterizing different-sized NPs in the aerosol.

3.2. RDD-spICP-MS for air-based aerosol measurements

100 nm AuNPs generated from a higher initial concentration of $5{\cdot}10^6$ #/mL were characterized with the same method when switching the gas phase to air with a broader DR range from 0.0002 to 0.06. With the increase of the DR, more air together with AuNP was brought into the plasma, which would not extinguish the plasma but degrade the sensitivity level. The single particle signal can still be well separated from the background, with the threshold at around 20 counts. As it is shown in Fig. 3a, the sensitivity of 100 nm AuNP decreased from around 1000 counts to 50 counts when DR was adjusted from 0.0006 to 0.06. However, with the increase of the DR, more particles were counted by spICP-MS. A linear relationship could be found between particle number and DR when the DR was below 0.033. This indicates that the setup can still characterize well particle numbers of metallic NPs in air-based aerosol despite the sensitivity loss. However, when $DR > 0.033$, the detected particle number was below the regression curve. On the one hand, the PNC may exceed the single particle measurement range, causing multiple NP events (Laborda et al., 2013). On the other hand, at higher DRs, the particle intensity was too close to the background level due to the sensitivity loss, thus a lot of particle signals would be regarded as the background. This observation is in agreement with the high LOD_{size} obtained for AuNPs in the air matrix. In this case, the LOD_{size} values for AuNPs were obtained using the internal Xe standard for correction at different DRs. As is shown in Fig. 3b, when selecting different DR, there was always a tradeoff between LOD_{size} and LOD_N. With the increase of the DR from 0.0006 to 0.033, the LOD_{size} increased from 25 nm to 78 nm. Meanwhile, the LOD_N decreased from 2500 #/L to 30 #/L. When $DR > 0.033$, the LOD_{size} is

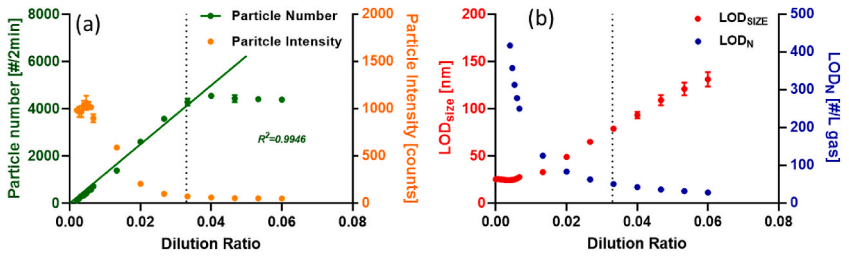

Fig. 3. (a) The median intensity (orange) and particle number (green) of 100 nm AuNP at each DR. (b) The LOD_{size} based on Xe signal correction (red) as well LOD_N at each DR. The dashed line indicates the boundary of the optimal DR working range. (For interpretation of the references to color in this figure legend, the reader is referred to the Web version of this article.)

close to or higher than 100 nm, where the particles cannot be distinguished from the background. Considering that the particle number at each DR was higher than LOD_N, we only need to consider the effect of LOD_{size}. The region where DRs below 0.033 was finally selected for 100 nm AuNPs characterization in the air matrix. The particle number concentration can be calculated back based on the slope of the linear curve found in Fig. 3 at $6.4{\cdot}10^4$ #/L gas.

Compared to the previous offline methods collecting NPs on filter collection followed by liquid extraction and spICP-MS characterization (Torregrosa et al., 2023), the LOD_N with our online setup was around 3000 times higher (0.01 #/L compared to our 30 #/L). This was mainly attributed to the much shorter measuring time with online mode compared to offline mode. However, even working in online mode, this LOD_N is still far below the recommended exposure limits of NP including AuNPs equal to $2{\cdot}10^7$ #/L in the air proposed by the UK, Germany, and the Netherlands (De Berardis et al., 2020). In addition, compared to other online setups using DMA or GED, the application of using RDD with Xe corrections can save more than 10 L/min argon and meanwhile decrease the LOD_N due to less dilution process in DMA (Myojo et al., 2002; Tan et al., 2016). These results showed that RDD-spICP-MS had great potential for metal characterization in ambient aerosol when considering the optimal DR to reach the requirements of both LOD_{size} and LOD_N.

3.3. RDD-spICP-MS for mixture sample measurements

3.3.1. Mixtures of different sized AuNPs

To test the size resolution capabilities of RDD-spICP-MS, various mixtures containing different-sized AuNPs were analyzed. As it is shown in Fig. 4 (a, b, and c), 40 nm AuNPs were mixed with 60, 80, and 100 nm AuNPs, respectively. In the mixtures containing 40 nm with 80 or 100 nm AuNPs, the peaks of the different sized particles were well separated. However, in the mixture of 40 nm with 60 nm AuNPs, there was an overlap in the PSD. A sum of two Gaussian distribution models was applied to run the deconvolution of the entire particle size distribution based on Equation (3).

$$N = N1 + N2 = A1 \times e^{-0.5\times\left(\frac{d-\mu 1}{\sigma 1}\right)^2} + A2 \times e^{-0.5\times\left(\frac{d-\mu 2}{\sigma 2}\right)^2} \quad \text{Equation 3}$$

where N is the particle number, N1 and N2 indicate the contributions of the 2 populations, and A1 and A2 are the amplitude of each

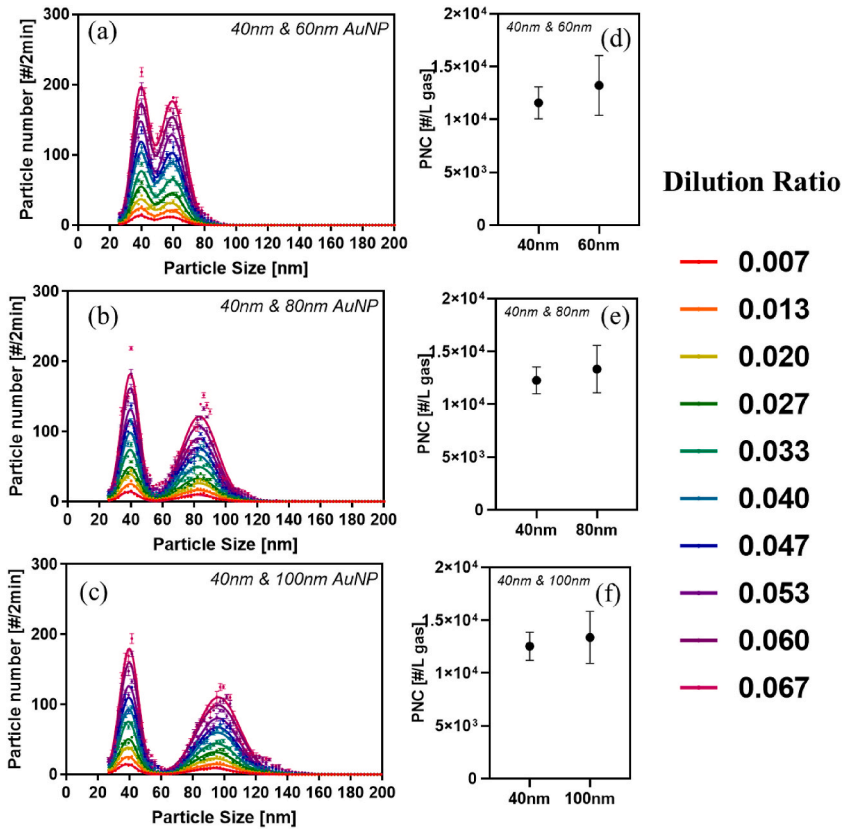

Fig. 4. PSDs and PNCs of 40 & 60 nm (a, d), 40 & 80 nm (b, e), and 40 & 100 nm (c, f) AuNPs at each nominal DR. The fitting curve (a, b, c) came from the sum of two Gaussian distributions and the PNCs (d, e, f) came from the deconvolution of each Gaussian distribution. Error bars stand for standard deviation (n = 3). *t*-test indicated no statistical difference in the PNC of each tested particle size in the mixture.

population; d is the particle size, μ1 and μ2 indicate the average size of the two peaks, and; σ1 and σ2 indicate the standard deviation of the N1 and N2.

As it is shown in Fig. 4 (a, b, and c), the original size distribution fits well with the sum of two Gaussian fittings. The parameters of A, μ, and σ of each population are shown in Fig. S4. With the increase of the DR, the A increases linearly, indicating the same online dilution trend as mono-sized particle samples. The stable μ and σ at each DR for both populations indicated the size distributions of the particles contained in the mixtures were not modified by the different DRs. After the separation of the two populations, an integration was applied to sum up the particle number of each population (N1 and N2). As it is shown in Fig. 4 (d, e, and f), in each mixture, the PNC of the 40 nm AuNP was always around $1.2{\cdot}10^4$ #/L gas, which was in agreement with the results obtained from the mono-sized experiments. The PNC of 60, 80, and 100 nm AuNPs was around $1.3{\cdot}10^4$ #/L gas. Compared to 40 nm AuNP, the standard deviation of PNC was larger for larger-sized particles. This may be due to the degree of fitting, where the larger-sized particles deviate more from the standard Gaussian distribution, increasing the error of the PNC calculation. The *t*-test results showed no statistical differences in the PNC between the two populations ($P > 0.05$) for each tested mixture. These results indicated that the aerosol containing different sized AuNPs can be well characterized by using the developed setup.

3.3.2. *Mixture of AuNPs with Au^{3+}*

Up to now, ionic interferences represent one of the limitations of spICP-MS in particular, for detecting small particles (Laborda et al., 2011; Torrent, Laborda, et al., 2019). For liquid samples, some methods have been proposed for distinguishing NPs from ionic interferences: 1) Dilution of the sample (Schwertfeger, Velicogna, Jesmer, Scroggins, & Princz, 2016); 2) Cloud point extraction for separating NPs from the ionic solution (Torrent, Laborda, et al., 2019; Wimmer et al., 2020, 2021); 3) Decrease the dwell time in spICP-MS (Abad-Álvaro et al., 2016); 4) Develop a more precise mathematic model for signal deconvolution (Cornelis & Hassellöv, 2014; Gundlach-Graham, Hendriks, Mehrabi, & Günther, 2018; Gundlach-Graham & Lancaster, 2022; Tuoriniemi, Cornelis, & Hassellöv, 2015). When extending these methodologies from liquid samples to aerosol samples, option 3) and 4) may be applied. The methods related to sample pretreatments are more difficult since they need to be worked online for aerosol samples. Moreover, the behavior of ionic interference in aerosol compared to liquid was not thoroughly investigated in previous studies. Fig. 5a compares the analysis in liquid and aerosol mode for mixtures containing elemental Au^0 from AuNPs and ionic Au^{3+} originating from $AuCl_3$. In liquid mode, the wet droplets are homogenously generated by concentric nebulizer containing Au^{3+} species and AuNPs. The concentration of the Au^{3+} in each droplet is equal to the concentration in the solution. Therefore, Au^{3+} gave a stable continuous signal during the analysis time. While in aerosol mode, the homogenous droplets generated from the aerosol generator containing Au^{3+} would form salt particles after drying. The size of the salt particles depends on the ionic concentration and initial droplet size. In addition, where the aerosol passes through the RDD, some small particles are lost due to the diffusion effect. This was confirmed during the RDD calibration (Fig. 2d). Therefore, in a mixture of AuNP/Au^{3+} at a 1:1 mass concentration ratio, the salt particles (black points at the bottom in

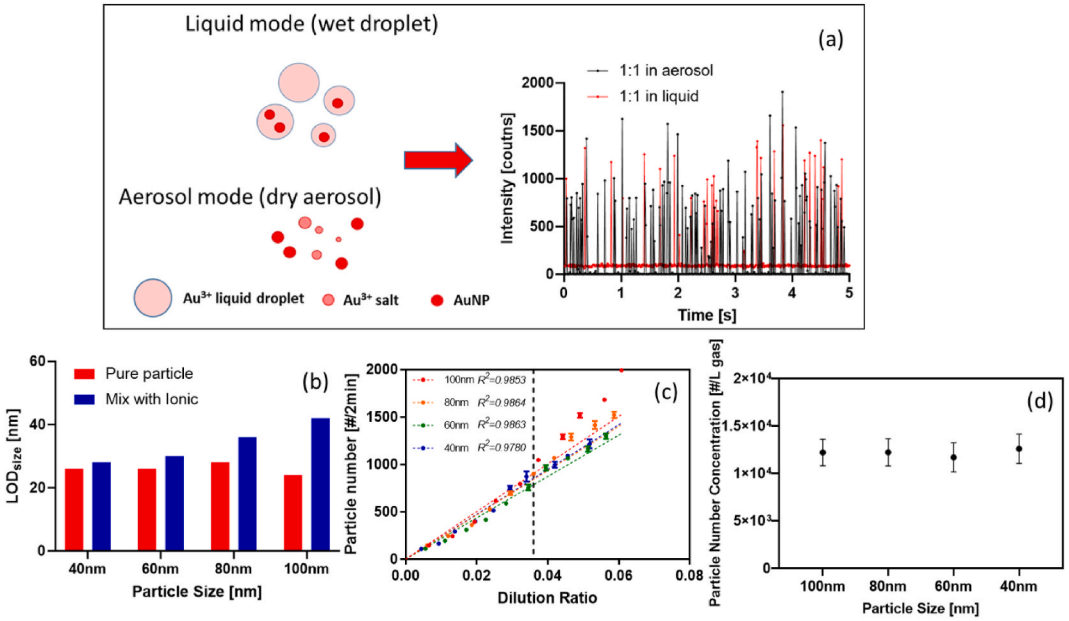

Fig. 5. (a) The time-resolved plot of 100 nm AuNPs mixed with the mass concentration equivalent Au^{3+} obtained from the analysis of standalone spICP-MS in liquid mode (red) and aerosol mode RDD-spICP-MS (black). (b) The LOD of pure particles (red bar) and the mixture of AuNPs with Au^{3+} at the equivalent gold mass concentration (blue bar). (c) The particle number of AuNPs at each DR. The dashed line indicates the boundary of the optimal DR working range. (D) The particle number concentration (PNC) of each sized AuNP in the aerosol. ANOVA test indicated no statistical difference in PNC among different sized AuNPs. (For interpretation of the references to color in this figure legend, the reader is referred to the Web version of this article.)

Fig. 5a) would not cause a continuous shift to higher intensities as it was in liquid mode (red points at the bottom in Fig. 5a).

To test if the coupled setup allows distinguishing NPs from the ionic interference, mixtures of 40, 60, 80, and 100 nm AuNPs with their equivalent Au^{3+} content were tested at different DRs, respectively. In all cases, no obvious shift was found for PSD (Fig. S5). Compared to the pure metallic AuNPs, i.e. in the absence of Au^{3+}, the LOD_{size} increases with increasing Au^{3+} concentration if mixed with larger-sized particles (Fig. 5b). To check the behavior of pure Au^{3+} in aerosol, the same experiments were repeated using pure Au^{3+} solutions to generate the aerosol, i.e. without AuNPs (Fig. S6). At all the mass concentrations selected, no ionic shift was observed in the time-resolved plot and there were signals at 0 count. When the signal was transferred into the histogram, for lower concentration Au^{3+} (40 or 60 nm equivalent Au^{3+}), most of the signals were below the LOD_{size} (dashed lines in Fig. S6). For higher concentration Au^{3+} (80 or 100 nm equivalent Au^{3+}), there were small amounts of the data points that exceeded the LOD_{size} at higher DR, presenting as a long tail in the histogram. These data would be misinterpreted as small particles during the AuNP characterization. However, when applying the online dilution of RDD towards lower DR, most of the data points could move towards the range below LOD_{size}.

This effect of ionic interference was also found when the particle numbers were counted from spICP-MS measurements. As shown in Fig. 5c, for small-sized AuNPs (40 and 60 nm), the particle numbers at each DR followed entirely a linear curve that passes through the origin. This indicated the optimal working range for all DR positions for smaller-sized AuNPs. For larger-sized AuNPs (80 nm and especially for 100 nm), the particle number started to deviate from the linear curve if DR $>$ 0.036. This deviation referred to the previous findings of pure Au^{3+} test. More Au^{3+} at high DR were misinterpreted as small particles. Therefore, in this case, the range when DR $<$ 0.036 is chosen as the optimal working DR for AuNP characterization to reduce the ionic interference. This was because the amount of the Au^{3+} particle generated from the droplet was much more than the number of AuNP. For AuNP, it always reaches the detector one by one, where the peak intensity depends on the particle mass. The online dilution only affect the peak frequency rather than the peak intensity. However, the Au^{3+} intensity depended on the salt particle mass as well as the particle number during each dwell time of the detection (Schwertfeger et al., 2016). Therefore, when applying a smaller DR, the peak of Au^{3+} would move towards a smaller intensity region until below the LOD_{size} to reduce the ionic interference.

When calculating back the initial number concentration in the aerosol, 100, 80, 60, and 40 nm AuNPs were all around $1.2{\cdot}10^4$ #/L gas without obvious difference checked by ANOVA test ($P > 0.05$, Fig. 5d). These results are at the same level compared to pure AuNP samples, indicating that the RDD could reduce the baseline ionic interference for spICP-MS measurements.

3.4. RDD-spICP-MS working in environmental aerosol matrices

Besides the ionic interference, non-spectral interferences from the sample matrix could affect the nanoparticle characterization in spICP-MS. For liquid suspension, previous studies have observed the NaCl decreased the peak intensity of As particles, meanwhile the presence of carbon could increase the peak intensity of these particles (Loula, Kaňa, & Mestek, 2019). The presence of the organics could affect the transport efficiency and the particle number (Torregrosa, Gómez-Pertusa, Grindlay, Gras, & Mora, 2022). Compared to

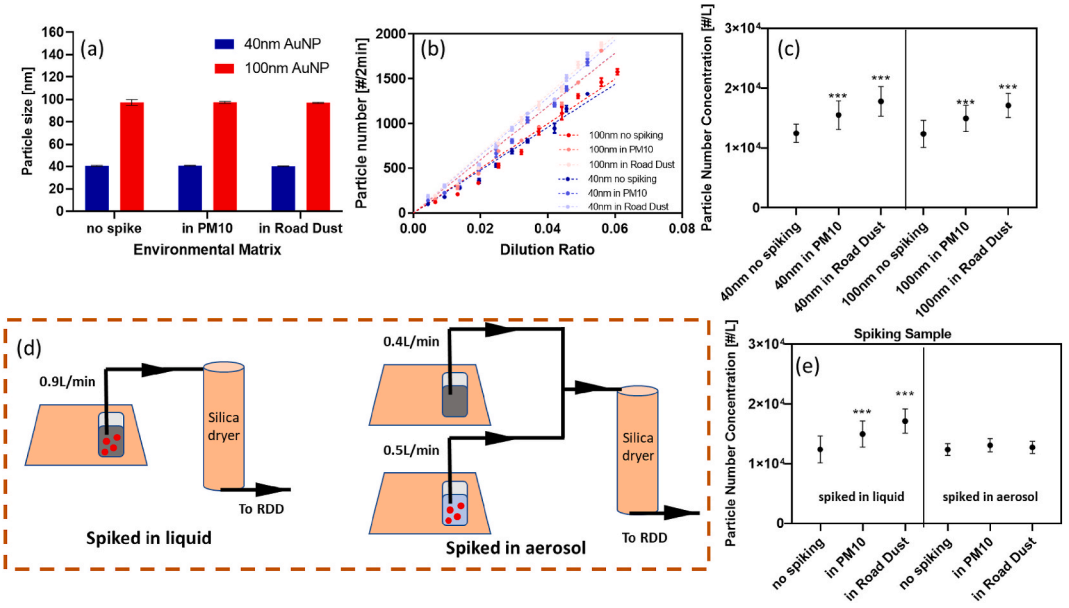

Fig. 6. (a) Particle size of 40 and 100 nm AuNPs under different spiking matrices. (b) Particle number of 40 and 100 nm AuNPs under different spiking matrices at different DR. (c) Particle number concentration of 40 and 100 nm AuNPs under different spiking matrices. ANOVA test indicated that none spiked samples were statistically different from spiked samples (***$P < 0.001$). (d) Different ways of spiking AuNPs with environmental matrix in liquid (left) and aerosol (right). (e) Particle number concentration of 100 nm AuNPs spiked with different environmental matrices in liquid (left) and aerosol (right).

liquid sample, the matrix effect in the aerosol is complicated as well especially for direct environmental sample analysis. To verify the capabilities of the RDD-spICP-MS working for complicated environmental aerosol matrices, Certified Reference Materials (CRMs) of road dust and PM10 were spiked with 40 and 100 nm AuNPs. The elemental composition of road dust and PM10 are presented in Tables S3 and S4 respectively. First of all, the aerosol of non-spiked road dust and PM10 suspensions were characterized by a scanning mobility particle sizer (SMPS), where the particle size of both samples was around 50 nm (Fig. S7). No obvious Au signal was detected in both matrices by spICP-MS (Fig. S8).

As shown in Fig. 6a, AuNPs of 40 and 100 nm spiked in road dust or PM10 suspensions, remained at the same size and corresponded to pure AuNPs (complete PSD in Fig. S9), indicating that these complex environmental matrices do not affect the determination of the particle size in the aerosol. Nevertheless, compared to pure AuNPs, the particle number at each DR increases after being spiked in road dust and PM10 suspensions (Fig. 6b), which obtains a larger slope of the linear fitting curve. This is further confirmed when calculating the PNC in the aerosol (Fig. 6c). The ANOVA test ($p < 0.001$) shows statistical differences between spiked and none-spiked samples. However, no obvious difference in PNC was found between the 40 nm and 100 nm samples for each spiked matrix.

The effect of the particle number shifting in environmental matrices was compared to the shift found with ionic interference in section 3.3.1. As shown before, the shift of the particle number at higher DR in the Au^{3+} mixture experiments comes from the misinterpretation of Au^{3+} as the smaller-sized AuNP. This interference could be reduced by online dilution when selecting smaller DR. This is because that dilution would not change the AuNP peak intensity position but Au^{3+} intensity distribution would move to the smaller intensity region which was below LOD_{size}. Therefore, in Fig. 5c, it is presented as a firstly linear but then a deviation of the particle towards a higher number. However, this is not the case for environmental matrices. As shown in Fig. S8, there was no obvious signal of Au found from the matrix, indicating it was not the effect of ionic interference. In addition, the shift of particle number happened in all DR but linearity ($R^2 > 0.98$) remains, giving a similar relative standard deviation level compared to the previous particle number concentration determination (error bar in Fig. 6c compared to **2f** and **5d**). Our interpretation is that the shift of the particle number came from the aerosol generation process, where the aerosol generator brought more AuNP from liquid suspension into the aerosol with the presence of environmental aerosol matrices. A previous study on non-spectral interferences in spICP-MS found that the presence of organics in liquid suspension could increase the transport efficiency of the particles due to the decrease of the surface tension (Torregrosa et al., 2022). This could be a possible reason to explain the shift of the particle number concentration since a huge amount of organic carbon was found in the environmental aerosol matrices in this study (Table S4).

To further validate this interpretation, a direct spiking of AuNP with environmental matrix in aerosol was applied compared to the previous spike in liquid (Fig. 6d). Compared to the previous aerosol generation from one bottle, in this aerosol spiking experiment, two bottles were used to generate AuNP and environmental matrix aerosol separately and then mixed before the dryer. When counting the particle number at different DRs, there was no obvious shift of the slope found with different environmental matrices (Fig. S10). When

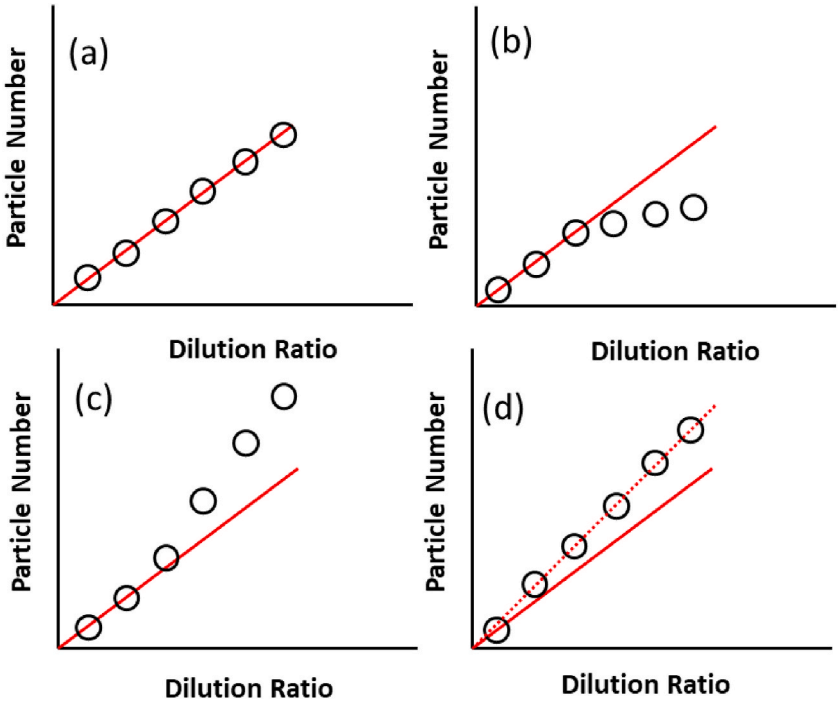

Fig. 7. Effects on linearity deviation when using RDD-spICP-MS for online dilution and particle counting. (a) Linear relationship between the PNC and the DR, when the PNC is the optimal for spICP-MS analysis. (b) Linearity is lost at high DR, where the particle number is underestimated. (c) Linearity is lost at high DR in presence of particles formed from ionic species. (d) Slope deviation as observed for the environmental samples tested in this study.

calculating the initial number concentration in the raw aerosol, there was no obvious difference in the number concentration at different spiking matrices in the aerosol according to the ANOVA test (Fig. 6e). This confirmed that the PNC shift comes from the aerosol generation step. When applying the RDD-spICP-MS for online measurement, the presence of an environmental matrix in the aerosol will not affect the particle characterization compared to the offline liquid measurements.

These results indicated the potential of RDD-spICP-MS in obtaining metallic NPs size and number characterization in complex environmental aerosol matrices. Compared to the liquid sample measurement, the presence of environmental matrices in the aerosol would not deviate from the particle number characterization.

3.5. Function of RDD in correcting spICP-MS characterization in different situations

In this paper, the coupling of RDD-spICP-MS is used to achieve online sampling, dilution, and characterization of the metallic NPs. RDD runs for online dilution based on the rotating speed and spICP-MS runs for counting based on the peak frequency. However, with different samples, the matrix effect will affect the relationship between particle number and dilution ratio as shown in different schemes in Fig. 7. Fig. 7a shows a typical case of the particle number obtained from an aerosol containing pure metallic NPs as Fig. 2e. In this case, the particle number follows linearity, the intercept passes through the origin and the slope of the curve represents the initial PNC in the raw aerosol before RDD dilution.

However, in some cases, the particle number deviating from the linearity at some DRs. As shown in Fig. 7b, the particle number at lower DR would follow the linearity of the DR, while in higher DR, the obtained particle number is lower than the expected number. This relates to the saturation of the detector because the sample is not properly diluted (two or more particles are counted as one particle), which is the case of Fig. 3a. In some cases, there would be a situation where particle number at lower DR follows the linearity of the DR, but at higher DR obtaining more particle number than expected as shown in Fig. 7c. This is due to the ionic interference, where at higher DR more ionic signal was misinterpreted as small particles, which was the case in Fig. 5c. Both situations above (Fig. 7b and c) can be corrected by the usage of RDD to obtain the initial particle number concentration when applying DR in optimal ranges.

In other cases the linearity remains at each DRs, while the slope between particle number and DR deviated as shown in Fig. 7d. The increase of the slope relates to an increase of the PNC in the raw aerosol due to a matrix effect in the aerosol generation. This is the case we found when the AuNPs analyzed in the presence of organics, with increase of the aerosol generation efficiency (Fig. 6b). In this case, the particle number counted by spICP-MS is correct but influenced by the matrix in the liquid. Therefore, RDD cannot correct the initial particle number concentration.

These results show that RDD is a powerful apparatus when coupled to spICP-MS. Based on adjusting different DRs, the working range of the spICP-MS is extended, and the interference can be compensated.

4. Conclusions

In this proof-of-concept study, an online system consisting of a rotating disk diluter and an ICP-MS, working in the single particle mode for sampling, diluting, and characterizing aerosol metallic NPs has been presented. The analysis of mono-sized AuNP aerosol demonstrated the capabilities of the developed setup for NPs characterization and quantification. The air-based aerosol analysis gave a insights about a prototype system for direct aerosol analysis. However, a sensitivity loss was observed due to the presence of air in the argon. The measurements can be corrected using Xe as an internal standard. The LOD was good enough to detect the particles at the concentration level requested by the regulations to avoid exposure risk. With the measurement of samples containing different sized AuNPs, the RDD-spICP-MS was able to distinguish the different types of NPs by using multi-Gaussian deconvolution. In addition, the linearity of the amplitude for different dilution ratios using the RDD indicates a high homogeneity of the mixtures containing different-sized particles. When mixing with Au^{3+}, more interference was observed at higher DR but was well reduced via online dilution with RDD. In the experiments in which environmental aerosol matrices were spiked with AuNPs, the particle sizes obtained by RDD-spICP-MS showed no difference among different matrices. A shift in particle numbers was found when spiking AuNP directly with environmental matrices in the liquid due to the effect on aerosol generation efficiency. When spiking the AuNP with environmental matrices in the aerosol, the PNC will not deviate. This indicated the presence of environmental matrices would not influence particle characterization directly in the aerosol. In all experiments, RDD played an important role in extending the spICP-MS PNC working range. These results indicate that RDD-spICP-MS has great potential for online environmental aerosol characterization based on its good LOD and performance of reducing interference. Future studies will expand the application of the developed setup to other metal and metal oxide NPs and to different natural and anthropogenic environments in which aerosols play a key role. Using an aerosol generator to provide aerosols is limited to insoluble NPs and may limit the size range in which particles can be investigated. However, the developed setup is highly versatile concerning different introduction systems for aerosol supply, including analytical systems, industrial processes, or natural samples.

Notes

The authors declare no competing financial interest.

Declaration of competing interest

The authors declare that they have no known competing financial interests or personal relationships that could have appeared to

influence the work reported in this paper.Andrea Testino reports financial support was provided by Swiss National Science Foundation - Project grant 184817.

Data availability

Data will be made available on request.

Acknowledgments

The authors would like to thank Zheyu Zhang (PSI) for supporting TEM measurements. Also, Yibo Zhao and Prof. Jing Wang (ETH Zürich) for providing the environmental samples and for the helpful discussions. This work was supported by the Swiss National Science Foundation [Grant number: SNF project 184817]. Support for equipment maintenance was also obtained from the Energy Systems Integration (ESI) Platform at PSI.

Appendix A. Supplementary data

Supplementary data to this article can be found online at https://doi.org/10.1016/j.jaerosci.2023.106283.

References

Abad-Álvaro, I., Peña-Vázquez, E., Bolea, E., Bermejo-Barrera, P., Castillo, J. R., & Laborda, F. (2016). Evaluation of number concentration quantification by single-particle inductively coupled plasma mass spectrometry: Microsecond vs. millisecond dwell times. *Analytical and Bioanalytical Chemistry, 408*(19), 5089–5097. https://doi.org/10.1007/s00216-016-9515-y

Abdolahpur Monikh, F., Chupani, L., Zusková, E., Peters, R., Vancová, M., Vijver, M. G., et al. (2019). Method for extraction and quantification of metal-based nanoparticles in biological media: Number-based biodistribution and bioconcentration. *Environmental Science and Technology, 53*(2), 946–953. https://doi.org/10.1021/ACS.EST.8B03715/SUPPL_FILE/ES8B03715_SI_001.PDF

Ayala, A., Olson, B., Cantrell, B., Drayton, M., & Barsic, N. (2003). Estimation of diffusion losses when sampling diesel aerosol: A quality assurance measure. *SAE Transactions*, 1656–1667.

Bacon, J. R., Butler, O. T., Cairns, W. R. L., Cavoura, O., Cook, J. M., Davidson, C. M., et al. (2022). Atomic spectrometry update – a review of advances in environmental analysis. *Journal of Analytical Atomic Spectrometry, 37*(1), 9–49. https://doi.org/10.1039/D1JA90054D

Bierwirth, M., Olszok, V., Wollmann, A., & Weber, A. P. (2022). A new coupling setup of DMA, CPC and sp-ICP-MS with increased versatility. *Journal of Aerosol Science, 163*, Article 105983.

Bilos, C., Colombo, J. C., Skorupka, C. N., & Rodriguez Presa, M. J. (2001). Sources, distribution and variability of airborne trace metals in La Plata City area, Argentina. *Environmental Pollution, 111*(1), 149–158. https://doi.org/10.1016/S0269-7491(99)00328-0

Bland, G. D., Battifarano, M., Liu, Q., Yang, X., Lu, D., Jiang, G., et al. (2022). Single-particle metal fingerprint analysis and machine learning pipeline for source apportionment of metal-containing fine particles in air. *Environmental Science and Technology Letters*. https://doi.org/10.1021/acs.estlett.2c00835

Bolea, E., Jimenez, M. S., Perez-Arantegui, J., Vidal, J. C., Bakir, M., Ben-Jeddou, K., et al. (2021). Analytical applications of single particle inductively coupled plasma mass spectrometry: A comprehensive and critical review. *Analytical Methods*, 2742–2795. https://doi.org/10.1039/d1ay00761k

Contado, C. (2015). Nanomaterials in consumer products: A challenging analytical problem. *Frontiers in Chemistry, 3*(AUG), 1–20. https://doi.org/10.3389/fchem.2015.00048

Cornelis, G., & Hassellöv, M. (2014). A signal deconvolution method to discriminate smaller nanoparticles in single particle ICP-MS. *Journal of Analytical Atomic Spectrometry, 29*(1), 134–144. https://doi.org/10.1039/c3ja50160d

Creamean, J. M., Neiman, P. J., Coleman, T., Senff, C. J., Kirgis, G., Alvarez, R. J., et al. (2016). Colorado air quality impacted by long-range-transported aerosol: A set of case studies during the 2015 pacific northwest fires. *Atmospheric Chemistry and Physics, 16*(18), 12329–12345.

De Berardis, B., Marchetti, M., Risuglia, A., Ietto, F., Fanizza, C., & Superti, F. (2020). Exposure to airborne gold nanoparticles: A review of current toxicological data on the respiratory tract. *Journal of Nanoparticle Research, 22*, 1–41.

Duelge, K. J., Mulholland, G. W., Bustos, A. R. M., Zachariah, M. R., & Pettibone, J. M. (2022). Improved accuracy for calibrated mass distribution measurements of bimetallic nanoparticles. *Journal of Aerosol Science, 165*, Article 106031.

Egorova, K. S., & Ananikov, V. P. (2017). Toxicity of metal compounds: Knowledge and myths. *Organometallics, 36*(21), 4071–4090. https://doi.org/10.1021/ACS.ORGANOMET.7B00605/ASSET/IMAGES/LARGE/OM-2017-006059_0014.JPEG

Flores, K., Turley, R. S., Valdes, C., Ye, Y., Cantu, J., Hernandez-Viezcas, J. A., et al. (2019). Environmental applications and recent innovations in single particle inductively coupled plasma mass spectrometry (SP-ICP-MS). *Applied Spectroscopy Reviews*, 1–26. https://doi.org/10.1080/05704928.2019.1694937, 0(0.

Foppiano, D., Tarik, M., Gubler Müller, E., & Ludwig, C. (2018a). Combustion generated nanomaterials: Online characterization: Via an ICP-MS based technique. Part I: Calibration strategy with a TGA. *Journal of Analytical Atomic Spectrometry, 33*(9), 1493–1499. https://doi.org/10.1039/c8ja00066b

Foppiano, D., Tarik, M., Gubler Müller, E., & Ludwig, C. (2018b). Combustion generated nanomaterials: Online characterization: Via an ICP-MS based technique. Part II: Resolving power for heterogeneous matrices. *Journal of Analytical Atomic Spectrometry, 33*(9), 1500–1505. https://doi.org/10.1039/c8ja00067k

Fuzzi, S., Baltensperger, U., Carslaw, K., Decesari, S., Denier van der Gon, H., Facchini, M. C., et al. (2015). Particulate matter, air quality and climate: Lessons learned and future needs. *Atmospheric Chemistry and Physics, 15*(14), 8217–8299.

Giannoukos, S., Lee, C. P., Tarik, M., Ludwig, C., Biollaz, S., Lamkaddam, H., et al. (2020). Real-time detection of aerosol metals using online extractive electrospray ionization mass spectrometry. *Analytical Chemistry, 92*(1), 1316–1325. https://doi.org/10.1021/acs.analchem.9b04480

Gundlach-Graham, A., Hendriks, L., Mehrabi, K., & Günther, D. (2018). Monte Carlo simulation of low-count signals in time-of-flight mass spectrometry and its application to single-particle detection. *Analytical Chemistry, 90*(20), 11847–11855. https://doi.org/10.1021/acs.analchem.8b01551

Gundlach-Graham, A., & Lancaster, R. (2022). Mass-dependent critical value expressions for particle finding in single-particle ICP-TOFMS. In *Analytical chemistry*. https://doi.org/10.1021/acs.analchem.2c05243

Guzman, K. A. D., Finnegan, M. P., & Banfield, J. F. (2006). Influence of surface potential on aggregation and transport of titania nanoparticles. *Environmental Science and Technology, 40*(24), 7688–7693. https://doi.org/10.1021/ES060847G/SUPPL_FILE/ES060847GSI20060817_115351.PDF

Hess, A., Tarik, M., Losert, S., Ilari, G., & Ludwig, C. (2016). Measuring air borne nanoparticles for characterizing hyphenated RDD-SMPS-ICPMS instrumentation. *Journal of Aerosol Science, 92*, 130–141. https://doi.org/10.1016/j.jaerosci.2015.10.007

Hess, A., Tarik, M., & Ludwig, C. (2015). A hyphenated SMPS-ICPMS coupling setup: Size-resolved element specific analysis of airborne nanoparticles. *Journal of Aerosol Science, 88*, 109–118. https://doi.org/10.1016/j.jaerosci.2015.05.016

Hineman, A., & Stephan, C. (2014). Effect of dwell time on single particle inductively coupled plasma mass spectrometry data acquisition quality. *Journal of Analytical Atomic Spectrometry, 29*(7), 1252–1257. https://doi.org/10.1039/c4ja00097h

Hotze, E. M., Phenrat, T., & Lowry, G. V. (2010). Nanoparticle aggregation: Challenges to understanding transport and reactivity in the environment. *Journal of Environmental Quality, 39*(6), 1909–1924. https://doi.org/10.2134/JEQ2009.0462

Hsieh, Y.-C., Lin, Y.-P., Hsiao, T.-C., & Hou, W.-C. (2022). A two-dimensional nanoparticle characterization method combining differential mobility analyzer and single-particle inductively coupled plasma-mass spectrometry with an atomizer-enabled sample introduction (ATM-DMA-spICP-MS): Toward the analysis of hetero. *Science of the Total Environment, 838*, Article 156444.

Hueglin, C., Scherrer, L., & Burtscher, H. (1997). An accurate, continuously adjustable dilution system (1:10 to 1:104) for submicron aerosols. *Journal of Aerosol Science, 28*(6), 1049–1055. https://doi.org/10.1016/S0021-8502(96)00485-5

Laborda, F., Jiménez-Lamana, J., Bolea, E., & Castillo, J. R. (2011). Selective identification, characterization and determination of dissolved silver(i) and silver nanoparticles based on single particle detection by inductively coupled plasma mass spectrometry. *Journal of Analytical Atomic Spectrometry, 26*(7), 1362–1371. https://doi.org/10.1039/c0ja00098a

Laborda, F., Jiménez-Lamana, J., Bolea, E., & Castillo, J. R. (2013). Critical considerations for the determination of nanoparticle number concentrations, size and number size distributions by single particle ICP-MS. *Journal of Analytical Atomic Spectrometry, 28*(8), 1220–1232. https://doi.org/10.1039/c3ja50100k

Loula, M., Kaňa, A., & Mestek, O. (2019). Non-spectral interferences in single-particle ICP-MS analysis: An underestimated phenomenon. *Talanta, 202*(March), 565–571. https://doi.org/10.1016/j.talanta.2019.04.073

Maurer-Jones, M. A., Gunsolus, I. L., Murphy, C. J., & Haynes, C. L. (2013). Toxicity of engineered nanoparticles in the environment. *Analytical Chemistry, 85*(6), 3036–3049. https://doi.org/10.1021/AC303636S/ASSET/IMAGES/AC303636S.SOCIAL.JPEG_V03

Meermann, B., & Nischwitz, V. (2018). ICP-MS for the analysis at the nanoscale-a tutorial review. *Journal of Analytical Atomic Spectrometry, 33*(9), 1432–1468. https://doi.org/10.1039/c8ja00037a. Royal Society of Chemistry.

Montaño, M. D., Badiei, H. R., Bazargan, S., & Ranville, J. F. (2014). Improvements in the detection and characterization of engineered nanoparticles using spICP-MS with microsecond dwell times. *Environmental Science: Nano, 1*(4), 338–346. https://doi.org/10.1039/c4en00058g

Moreno, T., Querol, X., Alastuey, A., Viana, M., Salvador, P., De la Campa, A. S., et al. (2006). Variations in atmospheric PM trace metal content in Spanish towns: Illustrating the chemical complexity of the inorganic urban aerosol cocktail. *Atmospheric Environment, 40*(35), 6791–6803.

Mozhayeva, D., & Engelhard, C. (2020). A critical review of single particle inductively coupled plasma mass spectrometry – a step towards an ideal method for nanomaterial characterization. *Journal of Analytical Atomic Spectrometry, 35*(9), 1740–1783. https://doi.org/10.1039/c9ja00206e

Myojo, T., Takaya, M., & Ono-Ogasawara, M. (2002). DMA as a gas converter from aerosol to "Argonsol" for real-time chemical analysis using ICP-MS. *Aerosol Science and Technology, 36*(1), 76–83. https://doi.org/10.1080/027868202753339096

Ohata, M., & Nishiguchi, K. (2017). Direct analysis of gaseous mercury in ambient air by gas to particle conversion-gas exchange ICPMS. *Journal of Analytical Atomic Spectrometry, 32*(4), 717–722. https://doi.org/10.1039/c6ja00292g

Ohata, M., Sakurai, H., Nishiguchi, K., Utani, K., & Günther, D. (2015). Direct analysis of ultra-trace semiconductor gas by inductively coupled plasma mass spectrometry coupled with gas to particle conversion-gas exchange technique. *Analytica Chimica Acta, 891*, 73–78. https://doi.org/10.1016/j.aca.2015.06.048

Pace, H. E., Rogers, N. J., Jarolimek, C., Coleman, V. A., Higgins, C. P., & Ranville, J. F. (2011). Determining transport efficiency for the purpose of counting and sizing nanoparticles via single particle inductively coupled plasma mass spectrometry. *Analytical Chemistry, 83*(24), 9361–9369. https://doi.org/10.1021/ac201952t

Petosa, A. R., Jaisi, D. P., Quevedo, I. R., Elimelech, M., & Tufenkji, N. (2010). Aggregation and deposition of engineered nanomaterials in aquatic environments: Role of physicochemical interactions. *Environmental Science and Technology, 44*(17), 6532–6549. https://doi.org/10.1021/ES100598H/SUPPL_FILE/ES100598H_SI_001.PDF

Quiterio, S. L., Sousa da Silva, C. R., Arbilla, G., & Escaleira, V. (2004). Metals in airborne particulate matter in the industrial district of Santa Cruz, Rio de Janeiro, in an annual period. *Atmospheric Environment, 38*(2), 321–331. https://doi.org/10.1016/J.ATMOSENV.2003.09.017

Rai, P., Furger, M., Slowik, J. G., Zhong, H., Tong, Y., Wang, L., et al. (2021). Characteristics and sources of hourly elements in PM10 and PM2. 5 during wintertime in Beijing. *Environmental Pollution, 278*, Article 116865.

Rodrigues, S. M., Trindade, T., Duarte, A. C., Pereira, E., Koopmans, G. F., & Römkens, P. F. A. M. (2016). A framework to measure the availability of engineered nanoparticles in soils: Trends in soil tests and analytical tools. *TrAC, Trends in Analytical Chemistry, 75*, 129–140. https://doi.org/10.1016/J.TRAC.2015.07.003

Schwertfeger, D. M., Velicogna, J. R., Jesmer, A. H., Saatcioglu, S., McShane, H., Scroggins, R. P., et al. (2017). Extracting metallic nanoparticles from soils for quantitative analysis: Method development using engineered silver nanoparticles and SP-ICP-MS. *Analytical Chemistry, 89*(4), 2505–2513. https://doi.org/10.1021/acs.analchem.6b04668

Schwertfeger, D. M., Velicogna, J. R., Jesmer, A. H., Scroggins, R. P., & Princz, J. I. (2016). Single particle-inductively coupled plasma mass spectroscopy analysis of metallic nanoparticles in environmental samples with large dissolved analyte fractions. *Analytical Chemistry, 88*(20), 9908–9914. https://doi.org/10.1021/acs.analchem.6b02716

Tan, J., Liu, J., Li, M., El Hadri, H., Hackley, V. A., & Zachariah, M. R. (2016). Electrospray-differential mobility hyphenated with single particle inductively coupled plasma mass spectrometry for characterization of nanoparticles and their aggregates. *Analytical Chemistry, 88*(17), 8548–8555. https://doi.org/10.1021/acs.analchem.6b01544

Tan, J., Yang, Y., El Hadri, H., Li, M., Hackley, V. A., & Zachariah, M. R. (2019). Fast quantification of nanorod geometry by DMA-spICP-MS. *Analyst, 144*(7), 2275–2283. https://doi.org/10.1039/c8an02250j

Tarik, M., Foppiano, D., Hess, A., & Ludwig, C. (2017). A practical guide on coupling a scanning mobility sizer and inductively coupled plasma mass spectrometer (SMPS-ICPMS). *Journal of Visualized Experiments, 125*, 1–9. https://doi.org/10.3791/55487, 2017.

Torregrosa, D., Gómez-Pertusa, C., Grindlay, G., Gras, L., & Mora, J. (2022). Organics non-spectral interferences on nanoparticle characterization by means of single particle inductively coupled plasma mass spectrometry. *Journal of Analytical Atomic Spectrometry, 38*(2), 403–413. https://doi.org/10.1039/d2ja00342b

Torregrosa, D., Grindlay, G., de la Guardia, M., Gras, L., & Mora, J. (2023). Determination of metallic nanoparticles in air filters by means single particle inductively coupled plasma mass spectrometry. *Talanta, 252*, Article 123818. https://doi.org/10.1016/j.talanta.2022.123818

Torrent, L., Laborda, F., Marguí, E., Hidalgo, M., & Iglesias, M. (2019). Combination of cloud point extraction with single particle inductively coupled plasma mass spectrometry to characterize silver nanoparticles in soil leachates. *Analytical and Bioanalytical Chemistry, 411*(20), 5317–5329. https://doi.org/10.1007/s00216-019-01914-y

Torrent, L., Marguí, E., Queralt, I., Hidalgo, M., & Iglesias, M. (2019). Interaction of silver nanoparticles with mediterranean agricultural soils: Lab-controlled adsorption and desorption studies. *Journal of Environmental Sciences, 83*, 205–216. https://doi.org/10.1016/j.jes.2019.03.018

Tuoriniemi, J., Cornelis, G., & Hassellöv, M. (2015). A new peak recognition algorithm for detection of ultra-small nano-particles by single particle ICP-MS using rapid time resolved data acquisition on a sector-field mass spectrometer. *Journal of Analytical Atomic Spectrometry, 30*(8), 1723–1729. https://doi.org/10.1039/C5JA00113G

Vance, M. E., Kuiken, T., Vejerano, E. P., McGinnis, S. P., Hochella, M. F., & Hull, D. R. (2015). Nanotechnology in the real world: Redeveloping the nanomaterial consumer products inventory. *Beilstein Journal of Nanotechnology, 6*(1), 1769–1780. https://doi.org/10.3762/bjnano.6.181

Wimmer, A., Urstoeger, A., Funck, N. C., Adler, F. P., Lenz, L., Doeblinger, M., et al. (2020). What happens to silver-based nanoparticles if they meet seawater? *Water Research, 171*, Article 115399. https://doi.org/10.1016/j.watres.2019.115399

Wimmer, A., Urstoeger, A., Hinke, T., Aust, M., Altmann, P. J., & Schuster, M. (2021). Separating dissolved silver from nanoparticulate silver is the key: Improved cloud-point-extraction hyphenated to single particle ICP-MS for comprehensive analysis of silver-based nanoparticles in real environmental samples down to single-digit nm particle. *Analytica Chimica Acta, 1150*, Article 238198. https://doi.org/10.1016/j.aca.2021.01.001

Zereini, F., Alt, F., Messerschmidt, J., Wiseman, C., Feldmann, I., Von Bohlen, A., et al. (2005). Concentration and distribution of heavy metals in urban airborne particulate matter in Frankfurt am Main, Germany. *Environmental Science and Technology, 39*(9), 2983–2989. https://doi.org/10.1021/es040040t

Zhao, Y.-B., Cen, T., Jiang, F., He, W., Zhang, X., Feng, X., et al. (2023). Aerosol-into-liquid capture and detection of atmospheric soluble metals across the gas–liquid interface using Janus-membrane electrodes. *Proceedings of the National Academy of Sciences, 120*(10), Article e2219388120. https://doi.org/10.1073/pnas.2219388120

Zhao, Y. B., Cen, T., Tang, J., He, W., Ludwig, C., Chen, S. C., et al. (2022). An elution-based method for estimating efficiencies of aerosol collection devices not affected by their pressure drops. *Separation and Purification Technology, 287*(December 2021), Article 120590. https://doi.org/10.1016/j.seppur.2022.120590

Zhao, J., Lin, M., Wang, Z., Cao, X., & Xing, B. (2020). Engineered nanomaterials in the environment: Are they safe? *Critical Reviews in Environmental Science and Technology*, 1–36. https://doi.org/10.1080/10643389.2020.1764279, 0(0.

Zhao, Y. B., Tang, J., Cen, T., Qiu, G., He, W., Jiang, F., et al. (2022). Integrated aerodynamic/electrochemical microsystem for collection and detection of nanogram-level airborne bioaccessible metals. *Sensors and Actuators B: Chemical, 351*, Article 130903. https://doi.org/10.1016/J.SNB.2021.130903